Journal of Atmospheric and Solar-Terrestrial Physics 148 (2016) 13–21

Contents lists available at ScienceDirect

Journal of Atmospheric and Solar-Terrestrial Physics

journal homepage: www.elsevier.com/locate/jastp

foF2 vs solar indices for the Rome station: Looking for the best general relation which is able to describe the anomalous minimum between cycles 23 and 24

L. Perna [a,b,*], M. Pezzopane [b]

[a] Università di Bologna "Alma Mater Studiorum", Viale Berti Pichat 6/2, 40126 Bologna, Italy
[b] Istituto Nazionale di Geofisica e Vulcanologia, Via di Vigna Murata 605, 00143 Roma, Italy

ARTICLE INFO

Article history:
Received 23 March 2016
Received in revised form
25 July 2016
Accepted 8 August 2016
Available online 9 August 2016

Keywords:
Mid-latitude ionosphere
Solar minimum cycle 23/24
Solar indices
foF2 modeling

ABSTRACT

Analyses of the dependence of the F2layer critical frequency, *fo*F2, on five widely used solar activity indices ($F_{10.7}$, *Lym-α*, *MgII*, *R* and $EUV_{0.1-50}$)are carried out considering noon values manually validated at the ionospheric station of Rome (41.8°N, 12.5°E, Italy) between January 1976 and December 2013, a period of time covering the last three solar cycles and including the prolonged and anomalous minimum of solar cycle 23/24 (years 2008–2009). After applying a 1-year running mean to both *fo*F2 and solar activity indices time series, a second order polynomial fitting proves to perform better than a linear one, and this is specifically due to the very low solar activity of the last solar minimum and to the remaining saturation effect characterizing the high solar activity. A comparison between observed and synthetic *fo*F2 values, the latter calculated by using the analytical relations found for every index, and some considerations made on the *R* parameter introduced by Solomon et al. (2013), suggest that *MgII* is the best index to describe the dependence of *fo*F2 on the solar activity. Three main reasons justify this result: (1) the good sensibility of *MgII* to the variations of *fo*F2 for low solar activity; (2) the reduced saturation effect characterizing *MgII* at high solar activity; (3) the poor influence of the hysteresis effect characterizing *MgII* at medium solar activity. On the other hand, the $F_{10.7}$ index, widely used as input parameter for numerous ionospheric models, does not represent properly the last minimum; specifically, it is not able to describe the variations of *fo*F2 under a solar activity level of $F_{10.7}=82\cdot10^{-22}$ [J Hz^{-1} s^{-1} m^{-2}].

1. Introduction

The terrestrial ionosphere is produced by the ionization of the neutral atmosphere caused by the solar radiation, and it is then expected to follow the Sun's behavior (e.g., Araujo-Pradere et al., 2011; Hargraves, 1995; Liu et al., 2006, 2011b; Solomon et al., 2010, 2013). The study of the relations between the main ionospheric characteristics and the indices of solar activity has recently increased because of the more accurate measurements of solar radiation in the ionospherically crucial Ultra Violet (UV, 120–400 nm) and Extreme Ultra Violet (EUV, 0.1–120 nm) bands.

Ionospheric trends have become a main subject of research since the beginning of nineties when they gained importance in the context of the global climatic change (Roble and Dickinson, 1989; Roble, 1995; Rishbeth, 1990; Rishbeth and Roble, 1992). Since then, a significant number of studies focussed on ionospheric trends and on their possible link with the middle and upper atmosphere cooling due to an increase of greenhouse gases (e.g., Ulich and Turunen, 1997; Danilov., 2012; Laštovička et al., 2012; Laštovička, 2013; Danilov and Konstantinova, 2015; Danilov, 2015; Scott and Stamper, 2015; Upadhyay and Mahajan, 1998; Hall and Cannon, 2002; Bremer et al., 2012; Mielich and Bremer, 2013; Qian et al., 2014; Cnossen and Franzke, 2014; Roininen et al., 2015).

The solar activity variations represent the most influent cause of the ionospheric characteristics observed variability. This is clearly shown by Fig. 1 where the 1-year running means of the solar radio flux at 10.7 cm ($F_{10.7}$), and of the F2 layer critical frequency (*fo*F2) observed at local noon at the ionospheric station of Rome (41.8°N, 12.5°E, Italy), are plotted for the time period from January 1976 to December 2013.

The analysis of relations (*fo*F2 vs *Solar Index*) is essential for two main reasons: (1) every ionospheric model is based on these relations; (2) possible signatures of the greenhouse effect on the ionosphere can be found only after an accurate cleaning of the ionospheric characteristic time series from solar activity (in particular) and geomagnetic dependences. As a consequence, the

* Corresponding author at: Università di Bologna "Alma Mater Studiorum", Viale Berti Pichat 6/2, 40126 Bologna, Italy.
E-mail addresses: luigi.perna@ingv.it (L. Perna), michael.pezzopane@ingv.it (M. Pezzopane).

http://dx.doi.org/10.1016/j.jastp.2016.08.003
1364-6826/

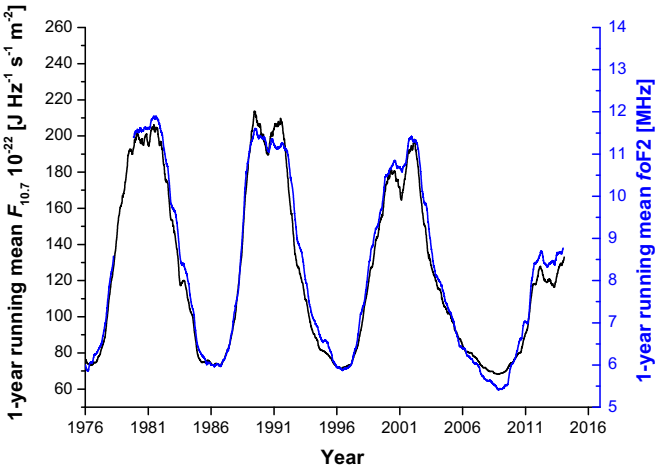

Fig. 1. 1-year running mean for both (black) $F_{10.7}$ and (blue) *fo*F2 noon values recorded at Rome ionospheric station, from the 1st January 1976 to the 31st December 2013. (For interpretation of the references to color in this figure legend, the reader is referred to the web version of this article.)

interest is particularly focused on analyzing whether these relations have been subjected to variations with solar cycles.

The last solar minimum, related to cycle 23/24 (years 2008–2009), was the longest and quietest period since the advent of space-based measurements (Liu et al., 2011a), and in many ways unusual: there were 527 spotless days for the two years 2008–2009, while they were respectively 226 and 176 for the minimum 22/23 (years 1996–1997) and 21/22 (years 1986–1987); the magnetic field at the solar poles was approximately 40% weaker than that of cycle 22/23 (Araujo-Pradere et al., 2011); measurements by the Ulysses spacecraft revealed a 20% drop in solar–wind pressure since the mid-1990s, the lowest point since the start of such measurements in the 1960s (Phillips, 2009). On the other hand, the Whole Heliosphere Interval (WHI), an internationally coordinated observing and modeling effort, reported that WHI solar–wind speed and radiation–belt flux were high compared to prior minima (Gibson et al., 2009). Under these particular conditions, the minimum of solar cycle 23/24 provides a perfect window to verify the relations between the main ionospheric characteristic *fo*F2 and the most widely used solar activity indices.

The solar EUV irradiance represents the main ionization source of the F2 ionospheric layer (e.g., Tobiska, 1996; Chen et al., 2012), explaining around 90% of the variance of characteristics such as *fo*F2 and *hm*F2 (e.g., Elias et al., 2014). Therefore, solar indices which refer to wavelengths in EUV band are the most appropriate to describe the ionospheric features. Virtually, none of the solar EUV and UV irradiance below 300 nm reaches the Earth's surface, therefore accurate measurements of EUV/UV irradiance must be made from above the terrestrial atmosphere. EUV continuous measurements started with the launch of the Solar Heliospheric Observatory (SOHO), only in late 1995 (Floyd et al., 2005). Furthermore, instruments used to perform measurements in these bands degrade because of intense UV and EUV exposure, and monitoring of this instrumental degradation is difficult; the spectral irradiances measured are consequently often afflicted by large uncertainties relative to the corresponding solar variation (Woods et al., 1996; Cebula et al., 1998).

For this reason, ionospheric models use different solar indices with longer dataset than the EUV one, and that can be considered good proxy for the general solar activity and for the EUV radiation in particular.

Chen et al. (2011, 2012) found a decrease of ~15% in the EUV solar radiation for the minimum of solar cycle 23/24 than respect to the previous one, which explains the lower values of *fo*F2 observed by ionospheric stations all around the world (Liu et al., 2011a; Chen et al., 2011; Bilitza et al., 2012). However, the considerable decrease characterizing the solar EUV radiation is quite different from that deduced from traditional solar EUV proxies such as the sunspots number *R* and $F_{10.7}$ (Elias et al., 2014). Furthermore, Emmert et al. (2010) and Chen et al. (2011) found that the long-term relation between the EUV irradiance and $F_{10.7}$ has changed markedly since around 2006, with EUV levels decreasing more than expected if compared to the $F_{10.7}$ index.

This discrepancy between EUV and widely used solar proxies such as *R* or $F_{10.7}$ can have very important consequences for the minimum of solar cycle 23/24. For instance, $F_{10.7}$ is widely used as the solar activity proxy by ionospheric and thermospheric models, such as the *IRI* (*International Reference Ionosphere*) model (Bilitza, 1989, 2001; Bilitza et al., 2014) and the *NRLMSISE-00* model (Picone et al., 2002).

Hence, in order to improve the efficiency of the ionospheric models, the research of a solar index that can approximate as reliably as possible the EUV radiation represents a priority in solar and ionospheric physics.

This work is focussed on the analysis of relations between *fo*F2 and five widely used solar activity indices: $F_{10.7}$, *Lym-α*, *MgII*, the sunspots number *R*, and the solar irradiance in the EUV band 0.1–50 nm ($EUV_{0.1–50}$). The study is based on the long and continuous *fo*F2 dataset recorded at the Rome ionospheric station between 1976 and 2013. The objectives of this study are mainly two: (1) to inspect the relations (*fo*F2 vs *Solar Index*) for the period January 1976–December 2013, looking for the best fitting one; (2) to search for the best index able to describe the variations of *fo*F2 both globally (for the complete dataset 1976–December 2013) and for the very particular conditions of the last solar minimum (for the time interval January 2008–December 2009). The datasets used are described in Section 2. Section 3 will explain the analysis carried out, and discuss the corresponding results. Conclusions are the subject of Section 4.

2. Data sources

2.1. Solar indices

$F_{10.7}$ is a solar proxy index that correlates quite well with the solar activity, in terms of EUV and X-ray emissions (Solomon et al., 2013). It has been extensively used in solar and upper atmosphere empirical models, such as IRI (Bilitza, 1989, 2001; Bilitza et al., 2014) and NRLMSISE-00 (Picone et al., 2002). It is continuously available from measurements obtained in Penticton, Canada, from which data for this flux have been given as daily values measured at local noon since 14 February 1947 (Covington and Medd, 1954). $F_{10.7}$ data have been downloaded from the database of the National Oceanic and Atmospheric Administration (NOAA) (http://www.ngdc.noaa.gov/stp/space-weather/solar-data/).

The hydrogen Lyman-α emission at 121.6 nm represents the strongest single line in the UV band, and has been measured for decades by rockets, the Atmosphere Explorer (AE) series of satellites, the Solar Mesosphere Explorer (SME), the Upper Atmosphere Research Satellite (UARS), the Thermosphere Ionosphere Mesosphere Energetics and Dynamics (TIMED), and the Solar Radiation and Climate Experiment (SORCE) missions (Solomon et al., 2013). A composite index, that was compiled by Woods et al. (2000), is based on a careful intercalibration of these measurements and the corresponding gaps are filled using correlation relations with $F_{10.7}$ and *MgII* indices. The dataset used in this work consists of a composite *Lym-α* index that integrates data from different satellite missions since 1947 and was downloaded from the Lasp Interactive Solar Irradiance Datacenter (LISIRD) database.

Detailed information about this composite dataset and free downloadable data are available at the website http://lasp.colorado.edu/lisird/composite_timeseries.html.

The core-to-wing ratio of the magnesium ion *h* and *k* lines at 279.56 and 280.27 nm is also a good indicator of the solar chromospheric activity, and is a useful proxy for solar irradiance in the UV and EUV wavelengths (Viereck et al., 2004, 2010). Called *MgII core-to-wing* index, it is calculated by taking the ratio between the highly variable chromospheric lines and the weakly varying photospheric wings (Solomon et al., 2013). As for the *Lym-α* index, the dataset is composite. *Mg II* data were downloaded from the free on-line database of Bremen University (http://www.iup.uni-bremen.de/gome/gomemgii.html), and are available from 07 November 1978.

The sunspots number *R* is the most widely used solar index, also because characterized by the longest dataset, with data available before the 1900. The daily values provided from SILSO (Sunspot Index and Long-term Solar Observations, Royal Observatory of Belgium, Brussels) database were considered (http://www.sidc.be/silso/datafiles).

Concerning the *Solar EUV* index, corresponding space-based observations include among others the Solar EUV Monitor (SEM) on SOHO (Judge et al., 1998), the Solar EUV Experiment (SEE) on TIMED satellite (Woods and Rottman , 2005), and the EUV Variability Experiment (EVE) on the Solar Dynamics Observatory (Woods et al., 2012). Nevertheless, only SEM has made measurements throughout the solar cycle 23 and during the last two solar minima in 1996–1997 and 2008–2009. SEM provides the integrated solar EUV flux in the two bands 0.1–50 nm and 26–34 nm, which contain the prominent 30.4 nm He II line and several coronal lines (Solomon et al., 2013). The two indices give comparable results. The one considered in this study is the $EUV_{0.1–50}$ index. Corresponding data are available as daily mean values from SOHO/SEM measurements since 01 January 1996, and were downloaded at the website http://www.usc.edu/dept/space_science/semdatafolder/semdownload.htm of the Space Sciences Center of the University of Southern California.

2.2. The F2-layer critical frequency foF2

*fo*F2 is the most important and used ionospheric characteristic, because it represents the maximum frequency that can be reflected by the ionosphere for an electromagnetic wave transmitted vertically.

In this work, the corresponding continuous and long–time dataset recorded at the Rome ionospheric station is considered. This dataset is composed by hourly validated values recorded from the 1st January 1976 to the 31st December 2013, hence covering the whole solar cycles 21, 22, 23 and the ascending phase of cycle 24. The values were validated according to the International Union of Radio Science (URSI) standard (Wakai et al., 1987), and in this work all the corresponding numerical values were considered independently of the presence of qualifying and descriptive letters. The validation was performed from traces recorded by classical ionosondes, which cannot tag the different polarization characterizing the two different modes of propagation of the electromagnetic wave. A VOS-1 chirp ionosonde produced by the Barry Research Corporation, Palo Alto, CA, USA (Barry Research Corporation, 1975) sounded from January 1976 to November 2004, and then it was replaced by an AIS-INGV ionosonde (Zuccheretti et al., 2003), for which the ionograms were validated by using the Interpre software (Pezzopane, 2004). This means that the *fo*F2 validated time series considered in this study represent a reliable and homogeneous data set.

Data were downloaded from the electronic Space Weather upper atmosphere database (eSWua; http://www.eswua.ingv.it/) (Romano et al., 2008).

3. Analysis and discussion

In this work, we refer to *fo*F2 values recorded at local noon (LT = UT + 1 h). This choice is suggested by the fact that for the considered solar indices the corresponding daily values in some cases derive from flows measured at local noon, as it is the case for the $F_{10.7}$ index and parts of composite datasets of *Lym-α* and *MgII*.

Before starting the analysis, a 1-year running mean for both *fo*F2 values and solar indices was performed. This is done because we are interested in finding the best relation between *fo*F2 and the solar activity, and the best way to accomplish this task is to "clean" the *fo*F2 time series from short-time ionospheric features, like those caused by geomagnetic disturbances, ionospheric seasonal and day-to-day variations (Liu et al., 2003, 2006, 2011a; Ma et al., 2009). In Fig. 1 the 1-year running mean for both $F_{10.7}$ and *fo*F2 noon values recorded in Rome, between January 1976 and December 2013, is plotted. The similarity of two curves is evident (the same is for all the other solar indices; the corresponding figures are not shown here), with no remarkable variations among different solar cycles. In the light of this similarity, as a first step, it is investigated whether a linear relation is suitable to properly describe the relation (*fo*F2 vs *Solar Index*), paying a particular attention on the last anomalous and prolonged solar minimum occurred in the years 2008–2009. It was decided to investigate first a linear relation because, when looking for long-term trends, this relation often is the one used to eliminate the solar activity influence (e.g., Ulich and Turunen, 1997; Upadhyay and Mahajan, 1998; Laštovička et al., 2006; Bremer, 2012; Laštovička et al., 2012; Mielich and Bremer, 2013; Cnossen and Franzke, 2014; Roininen et al., 2015).

According to this, a linear fit and the corresponding residuals analysis were performed for all the investigated relations, as shown in Fig. 2. The residuals analysis gives the possibility to make interesting additional considerations and to evaluate how much effects like the saturation and the hysteresis (Kane, 1992; Mikhailov and Mikhailov, 1995; Liu et al., 2006; Rao and Rao, 1969; Triskova and Chum, 1996) affect the relation (*fo*F2 vs *Solar Index*). It is worth noting that the analysis was done accordingly to Liu et al. (2011a), that is only the first smoothed (1-year running mean) value of each month, for both *fo*F2 and the solar index, is considered. Anyhow, a consistency test using the 15th smoothed value of each month has produced identical results.

Scatter plots between *fo*F2 and considered solar indices ($F_{10.7}$, *Lym-α*, *MgII*, *R*, and $EUV_{0.1–50}$), with the corresponding linear regression, are shown in the left column of Fig. 2; the red line represents the linear fit of data whereas blue, green and red dots indicate respectively the first smoothed value of each month for the minimum of solar cycle 21/22 (years 1986–1987), 22/23 (years 1996–1997), and 23/24 (years 2008–2009). The corresponding residuals analysis is shown in the right column of Fig. 2, where the residuals are plotted as a function of fitted *fo*F2 values, so that the horizontal black line corresponds exactly with the values of the linear fit. Red and brown dots indicate respectively residuals for data related to the last solar minimum and for data influenced by the remaining saturation effect. Orange dots in the (*fo*F2 vs $EUV_{0.1–50}$) scatter plots identify data related to the ascending phase of solar cycle 24 (from December 2010 to December 2013). The linear correlation coefficient *r* and the statistical parameter *Adj. R-square* (Appendix A) are specified in each of the residuals plot.

Focussing on *fo*F2 values recorded during the last solar minimum, Fig. 2 shows that these deviate from a linear fit. In particular, the deviation is quite significant for $F_{10.7}$, for which residuals are of the order of about 0.5 MHz, and less pronounced for *Lym-α*, *MgII*, *R* and $EUV_{0.1–50}$, for which residuals are of the order of about 0.25 MHz. Chen et al. (2011), studying the relation between 12-month mean *fo*F2 values (at 14 LT) and 12-month mean *P* values

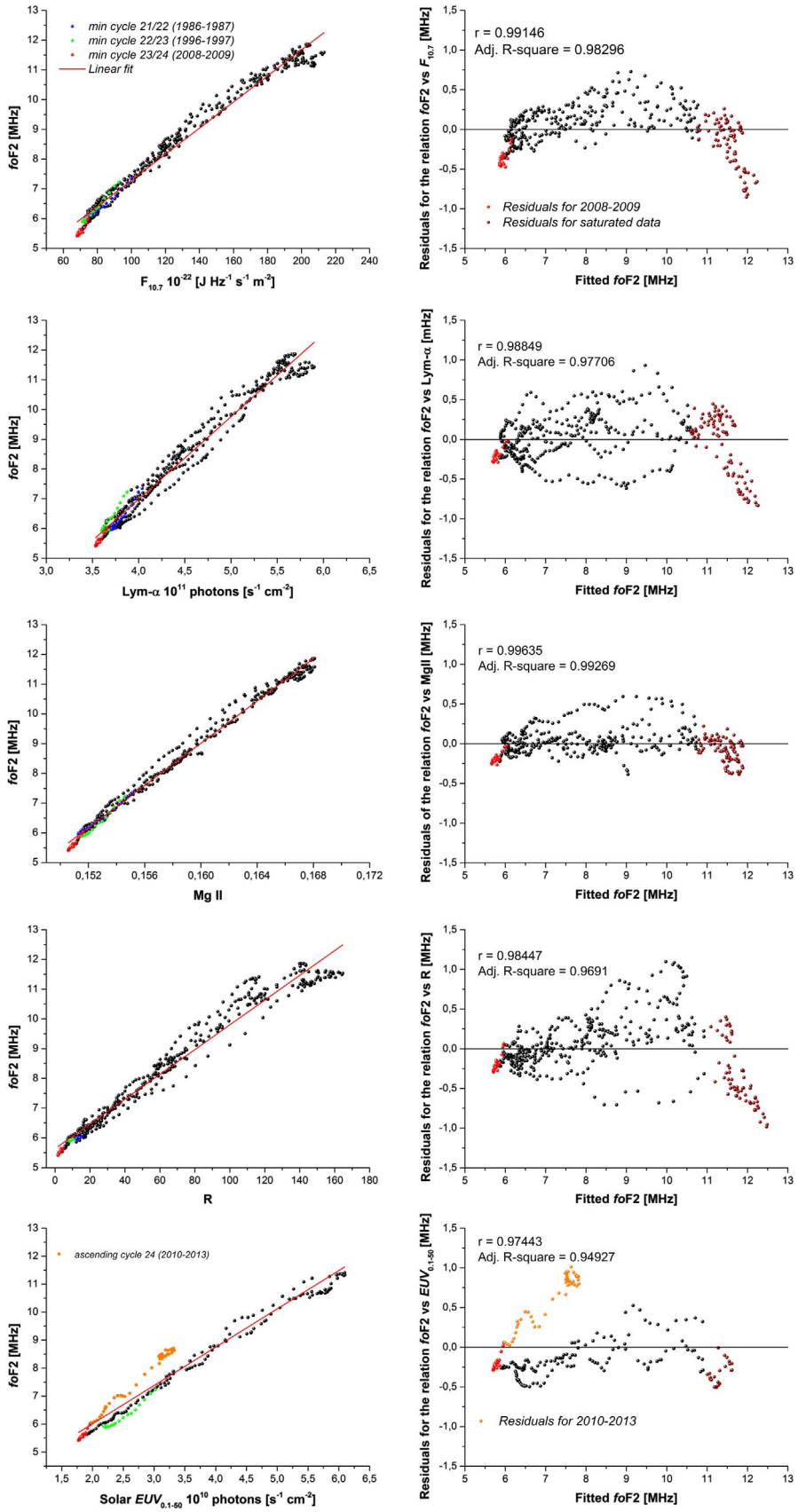

Fig. 2. (Left column) Scatter plots (*fo*F2 vs *Solar Index*) for indices $F_{10.7}$, *Lym-α*, *MgII*, *R* and $EUV_{0.1–50}$. Blue, green and red dots represent values for minima of solar cycles 21/22, 22/23 and 23/24 respectively. The linear fit of the whole dataset is highlighted by the red line. (right column) Residuals analysis of the linear fits. Red and brown dots represent respectively the residuals related to the last solar minimum and for data influenced by the remaining saturation effect. Orange dots in the scatter plots (*fo*F2 vs $EUV_{0.1–50}$) highlight the ascending phase of solar cycle 24 (January 2010 to December 2013). The linear correlation coefficient *r* and the statistical parameter *Adj. R-square* are also displayed. For both *fo*F2 and solar indices only the first smoothed (1-year running mean) value of each month is considered. (For interpretation of the references to color in this figure legend, the reader is referred to the web version of this article.)

(where $P=(F_{10.7}+F_{10.7A})/2$ and $F_{10.7A}$ is the 81-days running mean of $F_{10.7}$), found that the deviation from a linear approximation characterizing the last solar minimum shows a strong dependence on latitude. They observed that larger deviations characterize low latitude stations, in particular those close to the equatorial ionization anomaly, while very low deviations characterize mid latitude stations. Therefore, the low deviations observed in Rome are somewhat expected; the only one showing a rather significant unexpected deviation is that of $F_{10.7}$.

Some solar EUV irradiance models rely on the assumption that the relation between solar *EUV* indices and $F_{10.7}$ is invariant over different solar cycles (Chen et al., 2011). Fig. 2 shows that, for the last solar minimum, the relation (*fo*F2 vs $F_{10.7}$) shows a significant deviation from the linearity, while the values of previous minima (solar cycles 22/23 and 21/22) are still well represented by a linear fit. At the same time, Fig. 2 shows a better-conserved linearity for the relation (*fo*F2 vs $EUV_{0.1–50}$). These two results indicate a clear change in the relation between $F_{10.7}$ and $EUV_{0.1–50}$ for the last solar minimum. Moreover, Fig. 2 shows a clear non-random arrangement of residuals for $F_{10.7}$, which proves as a consequence that a linear fit is not a good indicator for this relation. Accordingly with Chen et al. (2011) and Solomon et al. (2013), it is possible to claim that $F_{10.7}$ cannot more be considered a good proxy for the radiation in the *EUV* wavelengths band.

At the same time, it is worth saying that if it is true that the linear fit of the (*fo*F2 vs $EUV_{0.1–50}$) relation is somewhat good for the last minimum, because of the short dataset characterizing $EUV_{0.1–50}$, a comparison with the previous minima cannot be done. So it is not possible to obtain information about possible changes of the relation (*fo*F2 vs $EUV_{0.1–50}$) for different solar cycles. Nevertheless, concerning $EUV_{0.1–50}$, Fig. 2 shows a huge deviation from the linearity for the ascending phase of solar cycle 24, a feature which is not observed for the other indices. This could be ascribed to a potential degradation of the SOHO/SEM instrument, which would cause a drift of solar measurements and a consequent overestimation of the $EUV_{0.1–50}$ irradiance (Chen et al., 2011; Wieman et al., 2014), even though Didkovsky et al. (2009) and Solomon et al. (2010) suggested that this effect is not overriding. Hence, for $EUV_{0.1–50}$, the slightly deviation of the linear fit from values related to the last solar minimum could also be due to this potential degradation, taking into account how the linear regression is affected by the dataset from January 2010 to December 2013. In fact, a linear fit done only on data from January 1996 to December 2009 describes very well the observed values for the last solar minimum (plot not shown here).

As already mentioned, the index $F_{10.7}$ is characterized by a non-random pattern of the residuals, which means that a linear fit cannot properly represent the relation (*fo*F2 vs $F_{10.7}$), independently of the solar activity. On the contrary, for the other indices a non-random distribution of the residuals is significantly observed only for high solar activity, because of the remaining saturation effect. This means that using a linear fit, *fo*F2 is highly overestimated for high solar activity, and the overestimation becomes more evident when monthly means or median values for both *fo*F2 and solar indices are considered (figures not shown here).

An important feature that can be studied using the residuals analysis is the spread of dots around the horizontal black line, which is particularly visible for medium solar activity (corresponding to *fo*F2 values from about 6.3–11 MHz), more markedly for *Lym-α* and *R* than for $F_{10.7}$, *MgII* and $EUV_{0.1–50}$. This spread is due to the hysteresis effect that causes two different values of *fo*F2 for the ascending and descending phases of a solar cycle, in correspondence of the same level of solar activity. As an example, Fig. 3 shows scatter plots (*fo*F2 vs *Lym-α*) for the ascending (full circles) and descending (open circles) phases of solar cycles 22 and

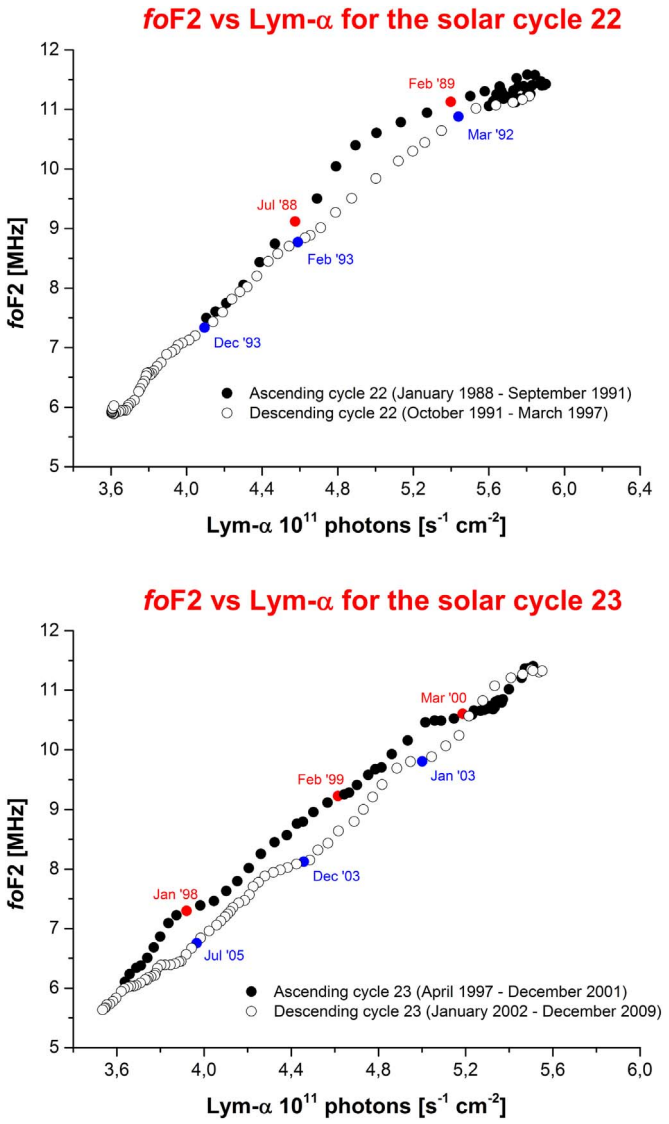

Fig. 3. Scatter plots (*fo*F2 vs *Lym-α*) for solar cycles 22 and 23. Full circles represent the ascending phase of the cycle whereas open circles represent the descending phase of the cycle. For both *fo*F2 and *Lym-α* only the first smoothed (1-year running mean) value of each month is plotted.

23. Mikhailov and Mikhailov (1995) postulated that the hysteresis is associated with differences in the geomagnetic activity during the ascending and descending phases of a solar cycle. Nevertheless, there is not yet an accepted explanation for the hysteresis effect (Liu et al., 2011b). The strong influence of the hysteresis effect is noticeable looking at the linear correlation coefficients *r* reported in the residuals plots of Fig. 2. The value of *r* is lower for *Lym-α* and *R*, that are affected by a clear hysteresis effect, and closer to one for those indices characterized by a lower hysteresis effect, namely *MgII* and $F_{10.7}$; the saturation effect and the particular values of the last solar minimum influence only marginally the value of *r*. Obviously, the hysteresis effect characterizing the medium solar activity strongly influences the search for the best index to describe the variation of *fo*F2. With regard to this, it is interesting to notice that the best linear correlation coefficient ($r\sim0.996$) is observed for the index *MgII*, that results to be less affected by both hysteresis and remaining saturation effect than the other indices.

By virtue of the previous considerations about both the extremely low solar activity of the last solar minimum and mostly the saturation at high solar activity, it is possible to claim that a

Table 1
Adj. R-square values, one for each solar index, for linear and quadratic fits of scatter plots (*fo*F2 vs *Solar Index*), considering the whole dataset January 1976–December 2013.

Solar Index	[Adj. R-square] (*fo*F2 vs *Solar Index*)$_{linear}$	[Adj. R-square] (*fo*F2 vs *Solar Index*)$_{quadratic}$
$F_{10.7}$	0.983	0.993
Lym-α	0.977	0.981
MgII	0.993	0.994
R	0.969	0.981
$EUV_{0.1–50}$	0.949	0.962

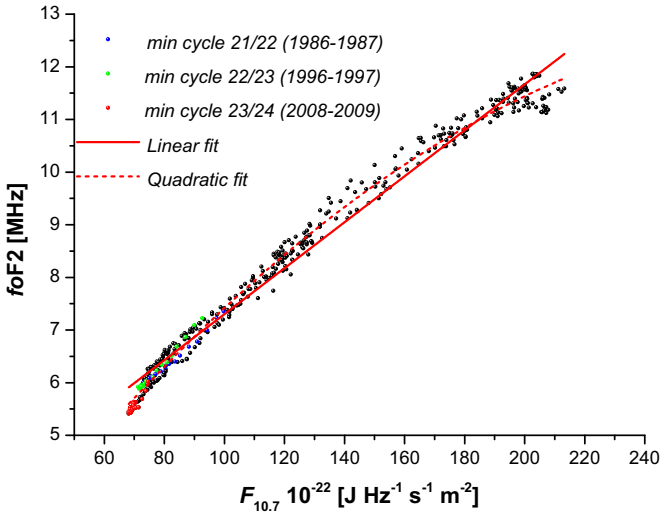

Fig. 4. (Solid red line) Linear fit and (dashed red curve) quadratic fit for the scatter plot (*fo*F2 vs $F_{10.7}$), for the whole period January 1976–December 2013. For both *fo*F2 and $F_{10.7}$ only the first smoothed (1-year running mean) value of each month is plotted. (For interpretation of the references to color in this figure legend, the reader is referred to the web version of this article.)

linear approximation cannot properly describe the relations (*fo*F2 vs *Solar Index*). A quadratic polynomial regression was then carried out, and Table 1 reports the values of the parameter *Adj. R-square* both for a linear and a quadratic fit, for each solar index. It is possible to notice that in every case there is an improvement of the fitting. This is essentially due to the fact that a quadratic fit can properly catch the deviation from the linearity due to both the remaining saturation effect and the very low solar activity of the last solar minimum. As an example, Fig. 4 shows the linear fit (red solid line) and the quadratic polynomial fit (red dashed line) for $F_{10.7}$.

In the wake of what it was done by other authors (Danilov and Mikhailov, 1999, 2001; Mikhailov and Marin, 2000, 2001; Ouattara, 2012; Danilov, 2015), higher-degree polynomial regressions were also tested, but the obtained results were practically identical to those obtained by a quadratic polynomial regression, confirming the results obtained by Kouris et al. (1998) and Liu et al. (2011b) who found that a higher-order polynomial does not improve significantly the fitting.

Concerning the quadratic relation, it is however important to stress the fact that it improves considerably the fitting for high solar activity and for the very low solar activity of the last solar minimum, but it cannot reduce the influence of the hysteresis effect. Further studies should take into account the possibility to use two different relations, one for the ascending phase of a solar cycle and the other one for the descending phase of a solar cycle. Once the quadratic approximation was chosen to represent the relation (*fo*F2 vs *Solar Index*), the following step consisted in looking for the corresponding best Solar Index. In order to

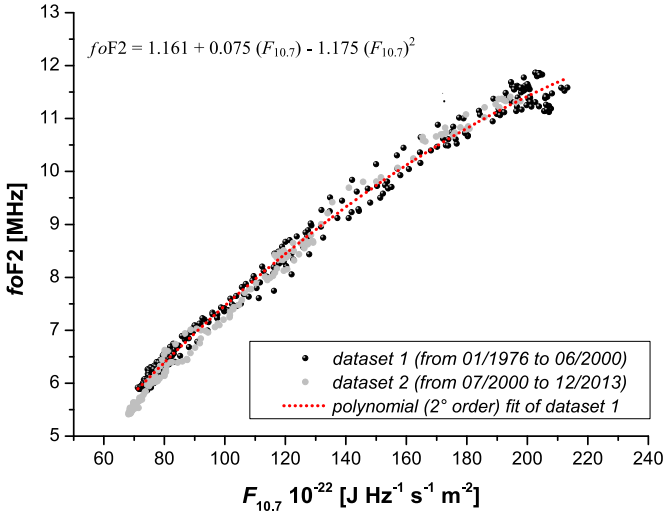

Fig. 5. Scatter plot of (*fo*F2 vs $F_{10.7}$). Black dots indicate data used for the fit (dataset 1, from January 1976 to June 2000), while gray dots indicate data excluded from the fit (dataset 2, from July 2000 to December 2013). The red dotted curve represents the quadratic fit of dataset 1. Only the first smoothed (1-year running mean) value of each month is plotted for both *fo*F2 and $F_{10.7}$. (For interpretation of the references to color in this figure legend, the reader is referred to the web version of this article.)

accomplish this task, two different approaches were considered and discussed, as it is described in the next two sections: (1) a comparison between observed and synthetic values of *fo*F2; (2) the calculation of the *R* parameter introduced by Solomon et al. (2013) for each of solar indices and *fo*F2.

3.1. Comparison between observed and synthetic values of foF2

Concerning synthetic *fo*F2 values, these were calculated for every index using analytical formulas that were obtained after fitting the relation (*fo*F2 vs *Solar Index*) with a quadratic relation, by considering only data from January 1976 to June 2000 (dataset 1). The time period between July 2000 and December 2013, including the descending phase of cycle 23, the anomalous minimum of solar cycle 23/24, and the ascending phase of cycle 24, was then considered as a validation window (dataset 2). Fig. 5 shows the two datasets and the quadratic fitting related to dataset 1 for the relation (*fo*F2 vs $F_{10.7}$). Table 2 summarizes for each index the analytical formulas related to dataset 1. Due to the short available dataset, this analysis is not carried out for the $EUV_{0.1–50}$ index, so no corresponding synthetic *fo*F2 values have been calculated.

Starting from these analytical relations, synthetic datasets of *fo*F2 (one for each solar index) were then generated for the period of dataset 2 simply introducing in them smoothed (1-year running mean) daily values of the solar index. These synthetic values were then compared with the observed ones.

Fig. 6 compares synthetic curves of *fo*F2 with the observed one at local noon in Rome. Looking at years of the last solar minimum, it is clear how the relation for $F_{10.7}$ gives an important

Table 2
Analytical formulas found by fitting scatter plots (*fo*F2 vs *Solar Index*), from January 1976 to June 2000, with a 2° order polynomial. *fo*F2 is expressed in [MHz], $F_{10.7}$ in [J Hz^{-1} s^{-1} m^{-2}], and *Lym-α* in [s^{-1} cm^{-2}].

Index	Quadratic regression (*fo*F2 vs *Solar Index*)$_{Jan76–Jun00}$
$F_{10.7}$	$foF2 = 1.161 + 0.075\ (F_{10.7}) - 1.175 \cdot 10^{-4}\ (F_{10.7})^2$
Lym–α	$foF2 = -10.55 + 5.676\ (Lym\text{-}\alpha) + 0.318\ (Lym\text{-}\alpha)^2$
MgII	$foF2 = 1.439 \cdot 10^2 + 1.568 \cdot 10^3\ (MgII) - 3.819 \cdot 10^3\ (MgII)^2$
R	$foF2 = 50.273 + 0.055\ (R) - 8.946 \cdot 10^{-5}\ (R)^2$

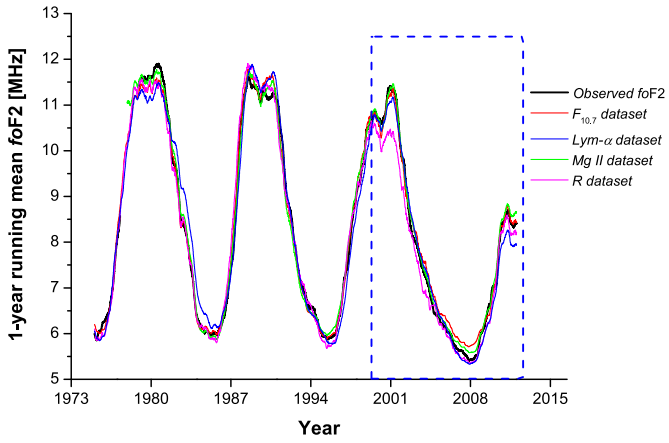

Fig. 6. (Black) 1-year running mean of the observed values of *fo*F2 recorded at local noon at Rome compared with synthetic values of *fo*F2 calculated using the quadratic relations shown in Table 2. The dashed blue box highlights the validation window between July 2000 and December 2013.

overestimation of the observed values, while a better correspondence is found for *MgII*, *Lym-α* and *R*. In addition, it is interesting to notice also the following features: (1) a significant underestimation of the maximum of solar cycle 23 (years 2000–2001) made by the *R* synthetic dataset; (2) an overestimation of the minimum of solar cycle 21/22 (years 1986–1987) made by the *Lym-α* synthetic dataset; (3) a poor representation of the descending phase of solar cycle 21 and of maximum phases of solar cycles 21/22 and 22/23 made by the *Lym-α* synthetic dataset; (4) an underestimation of the maximum of solar cycle 21 (years 1979–1980) related to the synthetic dataset of indices $F_{10.7}$, *Lym-α* and *R*.

To assess quantitatively the difference between synthetic and observed values of *fo*F2, the corresponding absolute deviation was calculated. Hence, by averaging the daily deviations, mean deviations $\left(\sum_{i=1}^{n}\left|foF2_{syn}-foF2_{obs}\right|_i/n\right)_{SI}=M_{SI}$ (where n is the number of values and SI stands for Solar Index) were then calculated for the following time periods: 1 January 2008–31 December 2009 (last solar minimum), 1 January 1976–31 December 2013 (whole dataset), and 1 July 2000–31 December 2013 (validation window). In this way, it is possible to understand what is the best solar index. The corresponding results are reported in Table 3, which shows that the good results characterizing the indices *Lym-α* and *R* for the last solar minimum, are not confirmed for the whole dataset. On the contrary, the acceptable result characterizing the index $F_{10.7}$ for the whole dataset is not confirmed for the last solar minimum. Specifically, $F_{10.7}$ seems to lose its sensibility for variations of *fo*F2 occurring under a specific solar activity level of approximately $82\cdot10^{-22}$ [J Hz^{-1} s^{-1} m^{-2}]. Overall, the best results are obtained for the *MgII* index, which can satisfactorily represent the *fo*F2 variations along all the considered solar cycles; this is mainly

Table 3

Mean absolute deviations $\left(\sum_{i=1}^{n}\left|foF2_{syn}-foF2_{obs}\right|_i/n\right)_{SI}=M_{SI}$ between observed and synthetic *fo*F2 values (where n is the number of values and SI stands for Solar Index), calculated by using analytical formulas shown in Table 2, for indices $F_{10.7}$, *Lym-α*, *MgII* and *R*, for the very low solar activity of years 2008–2009, for the whole dataset (1 January 1976–31 December 2013), and for the validation window (1 July 2000–31 December 2013).

Time period	$M_{F10.7}$	$M_{Lym-\alpha}$	M_{MgII}	M_R
2008–2009	0.248	0.140	0.121	0.104
1976–2013	0.577	0.678	0.446	0.644
Validation window (Jul 2000–Dec 2013)	0.169	0.252	0.126	0.282

because this is the index for which both the hysteresis effect and the saturation effect have the smallest impact; at the same time, the *MgII* index is characterized also by a good representation of the last solar minimum. The mean deviation values related to the validation window further confirm that the *MgII* is the best index to model the variations of *fo*F2.

3.2. The R parameter introduced by Solomon et al. (2013) to compare the variation of solar indices to that of foF2

In order to compare the variations of solar indices for the last two solar minima in a consistent way, Solomon et al. (2013) introduced the following parameter:

$$R=\frac{i(2008)-i(1996)}{i(2001)-i(1996)}, \quad (1)$$

where $i(\cdot)$ represents the annual average of the generic solar index i for the year indicated in brackets. Hence, the difference of the annual average value of each index in 2008 and 1996, that identify respectively minima of solar cycles 23/24 and 22/23, is divided by the expected solar cycle range of the index, as estimated by the difference between the annual average in the solar maximum year of 2001 and in 1996. The value of the *R* parameter found by Solomon et al. (2013) for each of solar indices is: $R_{F10.7}=-0.028$, $R_R=-0.056$, $R_{MgII}=-0.071$, $R_{Lym-\alpha}=-0.071$, and $R_{EUV}=-0.123$. A negative value of *R* means a lower value of the physical characteristics for the last solar minimum than for the previous one. With the aim to compare solar indices variations to that of *fo*F2, in addition to what was done by Solomon et al. (2013), the *R* parameter was calculated also for *fo*F2 obtaining $R_{foF2}=-0.074$, which is a value well correlated with those of *MgII* and *Lym-α*. Specifically, Table 4 reports the values of the *R* parameter for all the solar indices under investigation, and for *fo*F2, with the corresponding averages for years 2008 (minimum 23/24), 1996 (minimum 22/23) and 2001 (maximum cycle 23) used to calculate it. The most striking feature coming out from Table 4 is that the index $F_{10.7}$ confirms its poor ability to follow correctly the variations of *fo*F2 for low solar activity, especially those characterizing the anomalous and prolonged last solar minimum. Surprisingly, the *R* parameter for $EUV_{0.1-50}$ is quite higher than the one for *fo*F2. The reason could be found again in the potential degradation of the SOHO/SEM instrument. In particular, it is possible that an underestimation of the value for the year 2008 occurred, which means an overestimation made by the *R* parameter.

The fact that, according to the *R* parameter, *fo*F2 variations correlate well with those of *MgII* and *Lym-α* confirms what was found in the previous section and shown in Fig. 6, namely that in the period considered by the *R* parameter the *fo*F2 observed values are well represented by synthetic values related to both *MgII* and *Lym-α*.

Table 4

2008, 1996, 2001 averages and *R* parameter for all solar indices under investigation, and for *fo*F2 as measured at local noon at Rome.

Physical characteristic	2008 avg (min cycle 23/24)	1996 avg (min cycle 22/23)	2001 avg (max solar cycle 23)	*R* parameter
***foF2* (12 LT)** [MHz]	5.52	5.89	10.82	–0.07
$F_{10.7}$ 10^{-22} [J Hz^{-1} s^{-1} m^{-2}]	69.06	72.27	181.10	–0.03
Lym-α 10^{11} *phot* [s^{-1} cm^{-2}]	3.49	3.61	5.34	–0.07
MgII	0.1508	0.1516	0.1648	–0.06
R	2.85	8.63	111.00	–0.06
$EUV_{0.1-50}$ 10^{10} *phot* [s^{-1} cm^{-2}]	1.82	2.22	5.78	–0.11

Hence, the *R* parameter analysis suggests that *MgII* and *Lym-α* indices can be considered as the best candidates to obtain a reliable relation (*fo*F2 vs *Solar Index*). This result, combined with the one achieved in the previous section, suggests that *MgII* is the best index to describe the dependence of *fo*F2 on the solar activity.

4. Conclusions

The study of the relations between ionospheric characteristics and solar activity indices is of primary importance to improve ionospheric models. This paper considered five different solar indices ($F_{10.7}$, *R, MgII*, *Lym-α*, and $EUV_{0.1–50}$) and, relying on a long dataset of *fo*F2 values recorded at the ionospheric station of Rome between January 1976 and December 2013, showed that in order to properly approximate the relation (*fo*F2 vs *Solar Index*), a quadratic polynomial is better than a linear fit. In fact, the use of linear relations, widely utilized as input for both several ionospheric models and trend analyses, can cause a significant overestimation of observed data, mainly because of the saturation effect at high solar activity and the unusual low solar activities like the one that characterized the solar cycle 23/24.

Verified that a quadratic polynomial can suitably approximate the relation (*fo*F2 vs *Solar Index*), as a second step it was then shown that (*fo*F2 vs *MgII*) is the best relation to model the dependence of *fo*F2 on the solar activity. The main reasons of this outcome are: (1) a good sensibility of *MgII* to the variations of *fo*F2 for low solar activity; (2) a reduced saturation effect characterizing *MgII* at high solar activity; (3) a very slight hysteresis effect characterizing *MgII* for medium solar activity.

With regard to the other solar indices, the study showed that: a) at medium solar activity *Lym-α* and *R* are significantly affected by the hysteresis effect, and then it is important to pay particular attention when using analytical relations between *fo*F2 and these two indices; b) $F_{10.7}$ cannot properly follow the variations of *fo*F2 for the very anomalous minimum of solar cycle 23/24. In fact, for this solar minimum, synthetic *fo*F2 values calculated using $F_{10.7}$ are considerably overestimated with respect to the observed ones. It is then recommended to carefully use $F_{10.7}$ for low solar activity. In particular, a threshold of $82 \cdot 10^{-22}$ [J Hz^{-1} s^{-1} m^{-2}] below which *fo*F2 variations are no longer suitably reproduced was identified.

It is intention of the authors to consider the found quadratic relation (*fo*F2 vs *MgII*) for the Rome station to check whether the corresponding long-term trend of residuals $\Delta foF2 = foF2_{observed} - foF2_{synthetic}$ presents some signature due to greenhouse effects.

Appendix A. Adj. R-square

In order to get the final formula of the statistical parameter *Adj. R-square*, it is necessary to introduce the *summed square of residuals* (*SSE*) and the *coefficient of multiple determination* (*R-square*).

The *SSE* statistic parameter measures the total deviation between the observed values and the values predicted by the fit (synthetic values) of a physical quantity, and can be expressed by the following formula:

$$SSE = \sum_{i=1}^{n} w_i (y_i - \tilde{y}_i)^2, \tag{A.1}$$

where y_i represents the observed value while $\tilde{y}_i$ represents the synthetic value; w_i is the weight applied to each data point (usually $w_i = 1$). *SSE* close to zero indicates that the applied fit is good.

The *R-square* parameter gives information about how well the fit represents the variation of the observed dataset and can be expressed as:

$$R - square = 1 - \frac{SSE}{\sum_{i=1}^{n} w_i (y_i - \bar{y})^2}, \tag{A.2}$$

where $\bar{y}$ represents the average of the observed data. In this way the second term in (A.2) represents the ratio between *SSE* and the total sum of squares. *R-square* can assume any value between 0 and 1, with a value closer to 1 indicating that a greater proportion of variance is accounted for by the model.

It is now possible to introduce the *Adjusted R-square* that is a parameter that "adjusts" *R-square* based on the residual degrees of freedom and can be expressed as:

$$Adj.\ R - square = 1 - \frac{SSE}{\sum_{i=1}^{n} w_i (y_i - \bar{y})^2} \cdot \frac{(n-1)}{\nu}, \tag{A.3}$$

where ν represents the number of independent pieces of information involving the data points required to calculate the sum of squares (n). The parameter can assume any value from 0 to 1, with values closer to 1 that indicate a better fit. The *Adj. R-square* parameter is very useful and reliable if compared to *R-square*; in fact, the latter can increase just increasing the number of fitted coefficients, even without a real improve of the fit. This situation is avoided taking into account the degrees of freedom of the residuals.

References

Araujo–Pradere, E.A., Redmon, R., Fedrizzi, M., Viereck, R., Fuller–Rowell, T.J., 2011. Some characteristics of the ionospheric behavior during the solar cycle 23–24 minimum. Sol. Phys. 274, 439–456. http://dx.doi.org/10.1007/s11207–011–9728–3.

Barry Research Corporation, 1975. VOS-1A User Manual. Palo Alto, California, USA.

Bilitza, D., 1989. International Reference Ionosphere 1990. NSSDC 90-22, Greenbelt, Maryl, 53, 160. doi:10.1017/CBO9781107415324.004.

Bilitza, D., 2001. International Reference Ionosphere 2000. Radio Sci. 36, 261–275. http://dx.doi.org/10.1029/2000RS002432.

Bilitza, D., Brown, S. a, Wang, M.Y., Souza, J.R., Roddy, P. a, 2012. Measurements and IRI model predictions during the recent solar minimum. J. Atmos. Sol. Phys. 86, 99–106. http://dx.doi.org/10.1016/j.jastp.2012.06.010.

Bilitza, D., Altadill, D., Zhang, Y., Mertens, C., Truhlik, V., Richards, P., McKinnell, L.–A., Reinisch, B., 2014. The International Reference Ionosphere 2012 – a model of international collaboration. J. Space Weather Space Clim. 4, A07. http://dx.doi.org/10.1051/swsc/2014004.

Bremer, J., Damboldt, T., Mielich, J., Suessmann, P., 2012. Comparing long-term trends in the ionospheric F2-region with two different methods. J. Atmos. Sol. Phys. 77, 174–185. http://dx.doi.org/10.1016/j.jastp.2011.12.017.

Cebula, R.P., Deland, M.T., Hilsenrath, E., 1998. NOAA 11 solar backscattered ultraviolet, model 2 (SBUV/2) instrument solar spectral irradiance measurements in 1989–1994 1. Observations and long-term calibration. J. Geophys. Res. 103, 16235–16250.

Chen, Y., Liu, L., Wan, W., 2011. Does the F10.7 index correctly describe solar EUV flux during the deep solar minimum of 2007–2009? J. Geophys. Res. Space Phys. 116, 1–6. http://dx.doi.org/10.1029/2010JA016301.

Chen, Y., Liu, L., Wan, W., 2012. The discrepancy in solar EUV – proxy correlations on solar cycle and solar rotation timescales and its manifestation in the ionosphere. J. Geophys. Res. Space Phys. 117, 2–13. http://dx.doi.org/10.1029/2011JA017224.

Cnossen, I., Franzke, C., 2014. The role of the Sun in long-term change in the F2 peak ionosphere: new insights from EEMD and numerical modeling. J. Geophys. Res. Space Phys. 119, 8610–8623. http://dx.doi.org/10.1002/2014JA020048.

Covington, A.E., Medd, W.J., 1954. Variations of the daily level of the 10.7–centimetre solar emission. J. Radio Astron. Soc. Can. 48, 136.

Danilov, A.D., 2012. Long-term trends in the upper atmosphere and ionosphere: a review. Geomagn. Aeron. 52 (3), 271–291.

Danilov, A.D., 2015. Seasonal and diurnal variations in foF2 trends. J. Geophys. Res. Space Phys. 120, 3868–3882. http://dx.doi.org/10.1002/2014JA020971.

Danilov, A.D., Mikhailov, A.V., 1999. Long-term trends in the parameters of the F2 region: a new approach. Geomagn. Aeron. C/C Geomagn. Aeron. 39 (4), 473–479.

Danilov, A.D., Mikhailov, A.V., 2001. F2-layer parameters long-term trends at the Argentine Islands and Port Stanley stations. Ann. Geophys. 19 (3), 341–349.

Danilov, A.D., Konstantinova, A.V., 2015. Variations in *fo*F2 trends with season and local time. Geomagn. Aeron. 55 (1), 51–58.

Didkovsky, L., Judge, D., Wieman, S., McMullin, D., 2009. Minima of Solar Cycles 22/23 and 23/24 as Seen in SOHO/CELIAS/SEM Absolute Solar EUV Flux, Arxiv Prepr. arXiv0911.0870 6.

Elias, A.G., 2014. Filtering ionosphere parameters to detect trends linked to anthropogenic effects. Earth Planets Space 66, 113. http://dx.doi.org/10.1186/1880–5981–66–113.
Elias, A.G., Barbas, B.F.D.H., Shibasaki, K., Souza, J.R., 2014. Effect of solar cycle 23 in foF2. Trend Estim. Earth Planets Space 66, 111.
Emmert, J.T., Lean, J.L., Picone, J.M., 2010. Record–low thermospheric density during the 2008 solar minimum. Geophys. Res. Lett. 37, L12102. http://dx.doi.org/10.1029/2010GL043671.
Floyd, L., Newmark, J., Cook, J., Herring, L., McMullin, D., 2005. Solar EUV and UV spectral irradiances and solar indices. J. Atmos. Sol. Phys. 67, 3–15. http://dx.doi.org/10.1016/j.jastp.2004.07.013.
Gibson, S.E., Kozyra, J.U., de Toma, G., Emery, B.A., Onsager, T., Thompson, B.J., 2009. If the Sun is so quiet, why is the Earth ringing? A comparison of two solar minimum intervals. J. Geophys. Res. 114, A09105. http://dx.doi.org/10.1029/2009JA014342.
Hall, C.M., Cannon, P.S., 2002. Trends in foF2 above Tromso. Geophys. Res. Lett. 29. http://dx.doi.org/10.1029/2002GL016259.
Hargraves, R.B., 1995. The solar-terrestrial environment: an introduction to geospace. Q. J. R. Meteorol. Soc.
Judge, D.L., McMullin, D.R., Ogawa, H.S., Hovestadt, D., Klecker, B., Hilchenbach, M., Möbius, E., Canfield, L.R., Vest, R.E., Watts, R., Tarrio, C., Kühne, M., Wurz, P., 1998. First Solar EUV Irradiances Obtained from SOHO by the CELIAS/SEM, pp. 161–173.
Kane, R.P., 1992. Sunspots, solar radio noise, solar EUV and ionospheric foF2. J. Atmos. Terr. Phys. 54, 463–466.
Kouris, S.S., Bradley, P.A., Dominici, P., 1998. Letter to the editor: solar-cycle variation of the daily foF2 and M(3000)F2. Ann. Geophys. 16, 1039–1042. http://dx.doi.org/10.5194/angeo–16–1039–1998.
Laštovička, J., 2013. Trends in the upper atmosphere and ionosphere: recent progress. J. Geophys. Res. Space Phys. 118, 3924–3935. http://dx.doi.org/10.1002/jgra.50341.
Laštovička, J., Solomon, S.C., Qian, L., 2012. Trends in the neutral and ionized upper atmosphere. Space Sci. Rev. 168, 113–145. http://dx.doi.org/10.1007/s11214-011-9799-3.
Laštovička, J., Mikhailov, A.V., Ulich, T., Bremer, J., Elias, A.G., Ortiz de Adler, N., Jara, V., Abarca del Rio, R., Foppiano, A.J., Ovalle, E., Danilov, A.D., 2006. Long-term trends in foF2: a comparison of various methods. Ann. Geophys. 68, 1854–1870. http://dx.doi.org/10.1016/j.jastp.2006.02.009.
Liu, J.Y., Chen, V.I., Lin, J.S., 2003. Statistical investigation of the saturation effect in the ionospheric foF2 versus sunspot, solar radio noise, and solar EUV radiation. J. Geophys. Res. Space Phys. 108. http://dx.doi.org/10.1029/2001JA007543.
Liu, L., Chen, Y., Le, H., 2006. Solar activity variations of the ionospheric peak electron density. J. Geophys. Res. Space Phys. 113, 1–13. http://dx.doi.org/10.1029/2008JA013114.
Liu, L., Wan, W., Chen, Y., Le, H., 2011b. Solar activity effects of the ionosphere: a brief review. Chin. Sci. Bull. 56, 1202–1211. http://dx.doi.org/10.1007/s11434-010-4226-9.
Liu, L., Chen, Y., Le, H., Kurkin, V.I., Polekh, N.M., Lee, C.–C., 2011a. The ionosphere under extremely prolonged low solar activity. J. Geophys. Res. 116, A04320. http://dx.doi.org/10.1029/2010JA016296.
Ma, R., Xu, J., Wang, W., Yuan, W., 2009. Seasonal and latitudinal differences of the saturation effect between ionospheric NmF2 and solar activity indices. J. Geophys. Res. 114, A10303. http://dx.doi.org/10.1029/2009JA014353.
Mielich, J., Bremer, J., 2013. Long-term trends in the ionospheric F2 region with different solar activity indices. Ann. Geophys. 31, 291–303. http://dx.doi.org/10.5194/angeo-31-291-2013.
Mikhailov, A.V., Mikhailov, V.V., 1995. Solar cycle variations of annual mean noon foF2. Adv. Space Res 15, 79–82.
Mikhailov, A.V., Marin, D., 2000. Geomagnetic control of the foF2 long-term trends. Ann. Geophys. 18 (6), 653–665.
Mikhailov, A.V., Marin, D., 2001. An interpretation of the foF2 and hmF2 long-term trends in the framework of the geomagnetic control concept. Ann. Geophys. 19 (7), 733–748.
Ouattara, F., 2012. foF2 long term trends at Ouagadougou station. Br. J. Appl. Sci. Technol. 2 (3), 240–253.
Pezzopane, M., 2004. Interpre: a windows software for semiautomatic scaling of ionospheric parameters from ionograms. Comput. Geosci. 30, 125–130.
Picone, J.M., Hedin, a E., Drob, D.P., Aikin, a C., 2002. NRLMSISE-00 empirical model of the atmosphere: Statistical comparisons and scientific issues. J. Geophys. Res. 107, 1–16. http://dx.doi.org/10.1029/2002JA009430.
Qian, L., Solomon, S.C., Roble, R.G., 2014. Secular changes in the thermosphere and ionosphere between two quiet Sun periods. J. Geophys. Res. Space Phys. 119, 2255–2262. http://dx.doi.org/10.1002/2013JA019438.
Rao, M.S.J.G., Rao, R.S., 1969. The hysteresis variation in F2 – layer parameters. J. Atmos. Terr. Phys. 31, 1119–1125.
Rishbeth, H., 1990. A greenhouse effect in the ionosphere? Planet Space Sci. 38, 945–948.
Rishbeth, H., Roble, R.G., 1992. Cooling of the upper atmosphere by enhanced greenhouse gases. Modeling of the thermospheric and ionospheric effects. Planet Space Sci. 40, 1011–1026.
Roble, R.G., 1995. Major greenhouse cooling (yes, cooling): the upper atmosphere response to increased CO_2. Rev. Geophys. 33, 539–546.
Roble, R.G., Dickinson, R.E., 1989. How will changes in carbon dioxide and methane modify the mean structure of the mesosphere and thermosphere? Geophys. Res. Lett. 16, 1441–1444.
Roininen, L., Laine, M., Ulich, T., 2015. Time-varying ionosonde trend: case study of Sodankylä *hmF*2 data 1957–2014. J. Geophys. Res. Space Phys. 120, 6851–6859. http://dx.doi.org/10.1002/2015JA021176.
Romano, V., Pau, S., Pezzopane, M., Zuccheretti, E., Zolesi, B., Franceschi, G., De, Locatelli, S., 2008. The electronic space weather upper atmosphere (eSWua) project at INGV: advancements and state of the art. Ann. Geophys. 26, 345–351.
Scott, C.J., Stamper, R., 2015. Global variation in the long-term seasonal changes observed in ionospheric F region data. Ann. Geophys. 33, 449–455. http://dx.doi.org/10.5194/angeo-33-449-2015.
Solomon, S.C., Qian, L., Burns, A.G., 2013. The anomalous ionosphere between solar cycles 23 and 24. J. Geophys. Res. Space Phys. 118, 6524–6535. http://dx.doi.org/10.1002/jgra.50561.
Solomon, S.C., Woods, T.N., Didkovsky, L.V., Emmert, J.T., Qian, L., 2010. Anomalously low solar extreme – ultraviolet irradiance and thermospheric density during solar minimum. Geophys. Res. Lett. 37, L16103. http://dx.doi.org/10.1029/2010GL044468.
T., Phillips, 2009. Deep Solar Minimum [WWW Document]. NASA Sci. (URL) ⟨http://science.nasa.gov/science-news/science-at-nasa/2009/01apr_deepsolarminimum⟩.
Tobiska, W.K., 1996. Current status of solar EUV measurements and modeling. Adv. Sp. Res 18, 3–10. http://dx.doi.org/10.1016/0273-1177(95)00827-2.
Triskova, L., Chum, J., 1996. Hysteresis in dependence of *fo*F2 on solar indices. Adv. Space Res 18, 145–148.
Ulich, T., Turunen, E., 1997. Evidence for long-term cooling of the upper atmosphere in ionosonde data. Geophys. Res. Lett. 24, 1103–1106.
Upadhyay, H.O., Mahajan, K.K., 1998. Atmospheric greenhouse effect and ionospheric trends. Geophys. Res. Lett. 25, 3375–3378.
Viereck, R.A., Floyd, L.E., Crane, P.C., Woods, T.N., Knapp, B.G., Rottman, G., Weber, M., Puga, L.C., DeLand, M.T., 2004. A composite Mg II index spanning from 1978 to 2003. Space Weather 2, S10005. http://dx.doi.org/10.1029/2004SW000084.
Viereck, R.A., Snow, M., DeLand, M.T., Weber, M., Puga, L., Bouwer, D., 2010. Trends in solar UV and EUV irradiance: an update to the MgII index and a comparison of proxies and data to evaluate trends of the last 11-year solar cycle, in: Presented at 2010 Fall Meeting, AGU, San Francisco, Calif, Abstract GC21B-0877, 13–17 Dec.
Wakai, N., Ohyama, H., Koizumi, T., 1987. Manual of Ionogram Scaling. Ministry of posts and Telecommunications, Japan.
Wieman, S.R., Didkovsky, L.V., Judge, D.L., 2014. Resolving differences in absolute irradiance measurements between the SOHO/CELIAS/SEM and the SDO/EVE. Sol. Phys., 285–303. http://dx.doi.org/10.1007/978–1–4939–2038–9_18.
Woods, T., Prinz, D., Rottman, G., Al, E., 1996. Validation of the UARS solar ultraviolet irradiances: comparison with the ATLAS 1 and 2 measurements. J. Geophys. Res. 101, 9541–9569. http://dx.doi.org/10.1029/96JD00225.
Woods, T.N., Rottman, G., 2005. XUV photometer system (XPS): solar variations during the SORCE mission. Sol. Phys. 230, 375–387.
Woods, T.N., Tobiska, W.K., Rottman, G.J., Worden, J.R., 2000. Improved solar Lyman α irradiance modeling from 1947 through 1999 based on UARS observations. J. Geophys. Res. 105, 27195. http://dx.doi.org/10.1029/2000JA000051.
Woods, T.N., Eparvier, F.G., Hock, R., Jones, a R., Woodraska, D., Judge, D., Didkovsky, L., Lean, J., Mariska, J., Warren, H., McMullin, D., Chamberlin, P., Berthiaume, G., Bailey, S., Fuller–Rowell, T., Sojka, J., Tobiska, W.K., Viereck, R., 2012. Extreme ultraviolet variability experiment (EVE) on the solar dynamics observatory (SDO): overview of science objectives, instrument design, data products, and model developments. Sol. Phys. 275, 115–143. http://dx.doi.org/10.1007/s11207–009–9487–6.
Zuccheretti, E., Tutone, G., Sciacca, U., Bianchi, C., Arokiasamy, B.J., 2003. The new AIS-INGV digital ionosonde. Ann. Geophys., 46.